Optics Letters

Optical heterodyne detection system for a high-speed camera based on the HSA phase compensation method

Zengyan Wu, Changqing Cao,* Zhejun Feng, Xiaona Wu, and Chenxuan Duan

School of Optoelectronic Engineering, Xidian University, Xi'an 710071, China
**chqcao@mail.xidian.edu.cn*

Received 12 July 2023; revised 6 September 2023; accepted 6 September 2023; posted 7 September 2023; published 3 October 2023

This study proposes an innovative active optical heterodyne detection system to address the limitations of existing swarm intelligence algorithms in resolving phase compensation issues within coherent detection systems. The design incorporates a high-speed camera array detector, offering improved practicality and a simplified structure. Employing a heuristic search algorithm (HSA) transforms the high-dimensional problem into multiple one-dimensional optimization problems, significantly enhancing algorithmic running speed. The HSA maintains excellent performance even with increased array elements, allowing for real-time phase correction in large arrays. Experimental results using shot peening comparison samples reveal a substantial amplification of the heterodyne signal spectrum amplitude peak, approximately 60 times greater than the original signal. This innovative approach holds great potential for active optical heterodyne detection of dim targets, paving the way for further research in the field.

https://doi.org/10.1364/OL.500332

Optical signal detection encompasses direct and heterodyne methods, with heterodyne providing advantages [1]. By merging the signal and local laser on the detector's photosensitive surface, it converts signal data into an intermediate frequency (IF) signal, enhancing wavelength and frequency division multiplexing. [2]. However, heterodyne detection faces practical and technical challenges, including target characteristics, angle mismatch, polarization, and coherence. Interaction with rough surfaces causes modulation, creating speckle fields and distortion, leading to decoherence and reducing signal-to-noise ratio and efficiency [3]. These limitations constrain the engineering application of laser heterodyne detection [4].

Fink *et al.* proposed a scheme utilizing array detectors, demonstrating this approach's feasibility and theoretical underpinnings [5]. Subsequently, Chan *et al.* conducted heterodyne detection experiments using a 2×2 array detector, confirming its efficacy in improving the system's signal-to-noise ratio [6]. Dong *et al.* designed an array detector heterodyne detection system featuring a controllable mechanical photogate [7]. However, the traditional array detector heterodyne system relies on complex phase compensation modules, which hinder practicality and ease of operation. As a result, researchers have turned their attention to back-end algorithmic processing as an alternative to physical phase compensation modules [8]. While progress has been made in simplifying the system structure, the theoretical model for specific phase compensation schemes remains elusive. Liu *et al.* studied speckle effects in array detector heterodyne systems, creating a high-speed camera heterodyne system and validating the feasibility of adaptive particle swarm optimization (APSO) to mitigate these effects [4,9]. They proposed a spatial phase distortion compensation algorithm using parallel genetic algorithms [10,11]. Although the algorithm effectively compensates for decoherence, its real-time applicability is limited when handling substantial data volumes in global coherent lidar systems.

Thomson CSF Optronique company's researchers, including Clerc, demonstrated through experimentation that charge-coupled device (CCD) cameras can be utilized to record heterodyne detection signals [12]. Scientists from Yamagata University in Japan, led by Akiba, employed a heterodyne detection system with dual CCD cameras, utilizing frequency-synchronous detection techniques to obtain heterodyne signals under undersampling conditions [13,14]. Subsequently, due to the rapid advancement of optical coherence tomography (OCT) technology, CCD and CMOS cameras as heterodyne signal receivers have been extensively reported in the literature. This progress has prompted a reevaluation of array detector methods to overcome speckle effects in optical coherence detection.

This Letter presents an active optical heterodyne detection system using a high-speed camera-based array to address phase compensation challenges in coherent detection. The system offers a simplified structure and improved operability by utilizing the coherent interference signal generated on the camera sensor's photosensitive surface. To achieve real-time detection and overcome time delay issues, we propose the HSA spatial decoherence compensation algorithm, which significantly outperforms other algorithms in processing speed by 2–3 orders of magnitude. The algorithm exhibits a linear relationship with the number of detector array elements and is independent of the signal-to-noise ratio, ensuring exceptional real-time performance and stability. Experimental validation using shot peening comparison samples with varying roughness verifies the effectiveness of the phase compensation algorithm in mitigating

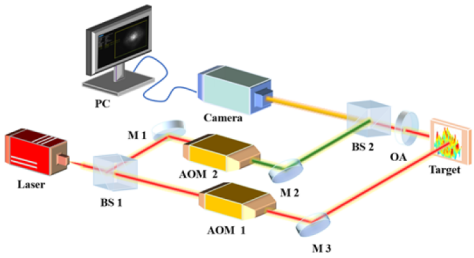

Fig. 1. Experimental device for active optical heterodyne detection system based on phase compensation algorithm scheme.

heterodyne detection signal decoherence caused by rough target surfaces and addressing wavefront distortion to a certain extent.

Figure 1 presents the experimental setup of a high-speed camera-based active optical heterodyne detection system, incorporating a phase compensation algorithm scheme, which does not require a hardware phase compensation module. Initially, a continuous-wave laser emits a laser beam with specific characteristics, including a central wavelength of 532.8 nm, a divergence angle of <0.5 mrad, and a linewidth of 5 MHz. The BS1 (beam splitter) divides the laser beam into local oscillator light (0.15 W) and signal light. For our experiment, we use high-speed cameras to mimic an array detector and complete the experimental setup. According to the Nyquist sampling theorem, a high-speed camera operating at a frame rate of 100 k fps can effectively capture signals with frequencies less than or equal to 50 kHz. However, it becomes evident that it cannot capture signals in the megahertz range even with a high-speed camera featuring a rapid image capture rate. Therefore, we proposed a dual-frequency shifting approach to overcome this limitation in our experiment. The local light is transmitted through M1 (mirror) into AOM1 (acoustic-optic modulator) for a frequency shift of 80 MHz, while AOM2 modulates the signal light with a frequency shift of 80.025 MHz. After AOM2 modulates the signal light and incident on the rough surface of the target through M3, the phase of the signal light wavefront is distorted. The spot size of the signal on the target is about 1 cm × 1 cm, and the optical power incident on the target is 80 mw. The reflected beam is concentrated through the OA optical antenna (OA) and irradiated on the BS2 (beam combiner) to mix with the local light coming through the M2 into the high-speed camera (Photron-FASTCAM NOVA S12) with a resolution of 128 × 96 and a sampling rate of 200 kHz. The high-speed camera captures and records the interference information, and the collected signal data is transmitted to a computer for real-time processing via a network cable. During acquisition, the front optical lens of the high-speed camera is removed to avoid interference.

In this study, heterodyne experiments were conducted to examine the impact of target surface roughness on optical heterodyne signals. Shot peening comparison samples with different roughness levels (quantified by Ra values of 0.2, 0.4, 0.8, and 1.6 μm) were used as detection targets after calibration with a specular target. Data analysis focused on 80 × 80 pixel units within the detection array. Figure 2 visualizes the heterodyne signals of targets with varying roughness, displaying the spectral distribution before algorithmic processing. The spot pattern with a roughness of 0.2 μm has the best quality. With the increase in roughness, the spot becomes dispersed and chaotic, decreasing heterodyne efficiency. The comparison sample block introduced severe decoherence effects, modulating the echo speckle field. This led to random phase differences within the locally detected

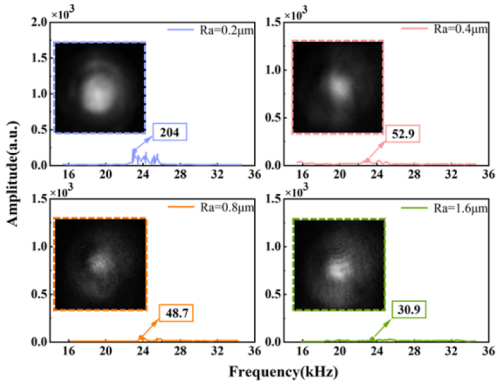

Fig. 2. Signal amplitude of different roughness targets before compensation.

oscillator signal across pixels, resulting in signal degradation in the presence of noise. Without phase compensation, the heterodyne signal-to-noise ratio substantially decreased, and there was a risk of no heterodyne signal output.

As in Ref. [8], we need to correct the output signal of each element of the array detector, and adding a phase to each element is equivalent to flattening the distortion in space, then:

$$\varphi(r) + \psi(i,j) = c, \tag{1}$$

where $\phi(r)$ represents the spatial phase at the position r of the intermediate frequency current signal, $\psi(i,j)$ is the additional phase of the i row and j column of the array, and c is the fixed constant. Therefore, by compensating for the output signals of all array elements, and ensuring that the total phases $\varphi(r) + \psi(i,j)$ of each detection unit are equal (both are constants C), the optimal detection efficiency can be achieved in the array detector heterodyne detection system. To achieve phase compensation for each array element, it is necessary to adjust the continuous sampling points over several cycles of each signal to ensure coherent superposition. Upon phase adjustment, the signals from the array detector are coherently combined, resulting in the expression of the obtained signal I_{SUM} after the following in-phase superposition:

$$I_{SUM} = \sum_{M}\sum_{N} I_{M,N}[\zeta_{M,N} : \kappa + \zeta_{M,N}], \quad \zeta_{M,N} \in \{1,2,\ldots,\rho\}\ . \tag{2}$$

Among them, $I_{M,N} = S_{M,N} + N_{M,N}$ represents the heterodyne signal containing noise output by the detector unit in row M and column N. For any element of the array detector, the heterodyne signal received by the detector can be expressed as $S_{M,N}$. The noise in heterodyne detection is mainly shot noise and thermal noise, so we use Gaussian white noise $N_{M,N}$ to characterize the noise signal. $\zeta_{M,N}$ represents the index value of the sampling point in the Mth row and Nth column, and ρ represents the number of sampling points in a single cycle, which is the ratio of the sampling rate to the frequency. $I_{M,N}[\zeta_{M,N} : \kappa + \zeta_{M,N}]$ represents the continuous κ sampling data for this array element starting from the point $\zeta_{M,N}$. This approach enables phase compensation, effectively addressing wavefront distortion. The next challenge is to identify a suitable set of $\zeta_{M,N}$ values. Typically, the intermediate frequency is known during heterodyne detection. In the absence of wavefront distortion, the heterodyne signal's amplitude should be maximized at the center frequency. Therefore, the spectrum analysis of the total signal I_{SUM} of the adjusted

array detector is carried out:

$$F = |FFT(I_{SUM})|. \tag{3}$$

Taking the maximum signal amplitude at the intermediate frequency as the objective function, the above problem can be transformed into an optimization problem, namely

$$\begin{aligned} \max \quad & F_{IF}\ (M,N) \\ s.t. \quad & \zeta_{M,N} \in \{1,2,\ldots,\rho\} \end{aligned} \quad . \tag{4}$$

The amplitude $F_{IF}(M,N)$ at the intermediate frequency signal, which is the sum of the phase-adjusted array element signal in Mth and Nth column, plays a crucial role in this sub-problem. Since the dimension of this sub-problem's solution is 1, there is no need to consider other signals from the adjusted array elements during the calculation. Consequently, one array element can be randomly selected for compensation, and the phases of the other array elements can be adjusted to match that of the selected element. This forms the fundamental principle of the heuristic search algorithm (HSA). In the HSA, an array element is randomly chosen, and a phase is randomly assigned to its signal. The following array element is then selected, and a one-dimensional search algorithm is employed to determine the adjustment value that aligns its phase with the previous array element signal. The two signals are combined after the adjustment. This process continues, ensuring that each array element's phase is in synchronization with the signal obtained previously until all array element phase adjustments are determined.

This study compares the effectiveness of the HSA spatial decoherence compensation algorithm with three swarm intelligence algorithms: the particle swarm optimization (PSO) [8], adaptive particle swarm optimization (APSO) [8], and genetic algorithm (GA) [9]. Evaluations include algorithm processing effects, time costs, stability, and related factors. Swarm intelligence algorithms simulate collective behaviors observed in nature and exhibit distinct characteristics. The simulation involves a system with nine array detector elements, a 100 Hz heterodyne intermediate frequency signal, and a 3 s sampling duration at a 1000 Hz sampling rate. Each array element has a signal amplitude of 1, a −10 dB signal-to-noise ratio, and an initial phase following a uniform distribution. APSO and GA employ 100 iterations and an initial population of 200 to ensure fitness function convergence.

Figure 3(a) presents the amplitude of the intermediate frequency signal obtained after 100 iterations of the four optimization algorithms under a signal-to-noise ratio of −10 dB. The GA algorithm achieved an average amplitude of 9.3248 with a variance of 0.0048 and an average running time of 1.645 s. The PSO algorithm had a slightly slower average running time of 1.98 s, with an average amplitude of 9.195 and a variance of 0.023. APSO exhibited an average running time of 2.86 s, an average amplitude of 8.775, and a variance of 0.11. However, APSO's adaptive weight calculation reduced computational performance and convergence speed, making it less effective than the other two algorithms. In contrast, the proposed HSA algorithm achieved significantly faster processing with an average running time of 0.0031 s, outperforming swarm intelligence optimization algorithms, and is 530 times faster than GA. Regarding accuracy, the HSA algorithm attained an average amplitude of 9.4615, and its amplitude variance (0.001) was lower than that of the swarm intelligence optimization algorithms.

Heterodyne efficiency [4], a crucial metric for assessing phase matching, was evaluated for four algorithms. Figure 3(b) illustrates the heterodyne efficiency of the solutions obtained by the four algorithms. The GA algorithm demonstrated a mean heterodyne efficiency of 0.9941 with a variance of 0.0004, indicating stability and effective problem-solving capabilities with nine array elements. PSO yielded a slightly lower mean heterodyne efficiency of 0.988 with a variance of 0.0005, suggesting limitations in terms of iterations and particle swarm size. APSO achieved an average heterodyne efficiency of 0.886 with a variance of 0.005. The proposed HSA algorithm exhibited a higher mean heterodyne efficiency of 0.9947 and superior stability, with a lower variance (3.4235×10^{-6}) than swarm intelligence optimization algorithms. Comparing the proposed algorithm with GA, both demonstrated similar compensation effects and stability, outperforming APSO. However, the GA algorithm was limited by its slow operation speed and constraints on the number of array elements.

Figure 4(a) displays the operation time comparison between the GA and HSA algorithms as the number of array elements increases. Ten sets of data were generated for each element number, and the average value was calculated over 100 iterations. The GA algorithm initially exhibits fast running times, but as the number of array elements reaches 80, the running time increases to approximately 40 s, deviating from a linear relationship. This suggests that the GA algorithm may face challenges when dealing with a large number of array elements directly. Conversely, the HSA algorithm demonstrates a linear relationship between the number of elements and running time, with a correlation coefficient of 0.9949. The average processing time per element is only 0.0004 s, enabling real-time processing even with 300 array elements (running time is 0.125 s). Figure 4(b) illustrates the heterodyne efficiency trends as the number of array elements increased. The GA efficiency gradually decreases, indicating limitations in handling the exponential solution space growth. In contrast, HSA maintains high efficiency, regardless of the number of elements, even at a signal-to-noise ratio of −10 dB.

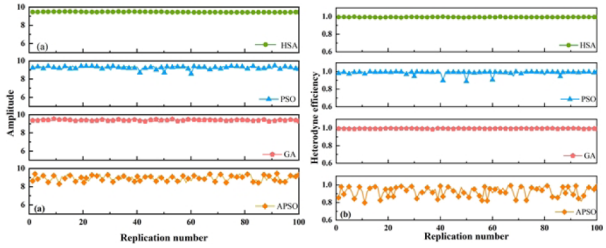

Fig. 3. Comparison of HSA algorithm and GA algorithm, PSO algorithm, and APSO algorithm operation results: (a) signal amplitude; (b) heterodyne efficiency.

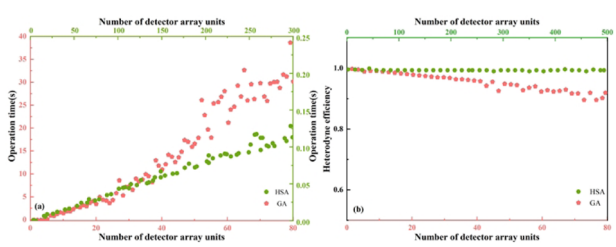

Fig. 4. (a) Operation time and (b) heterodyne efficiency of GA algorithm and HSA algorithm changes with the number of array elements.

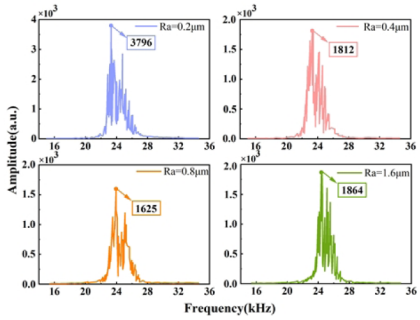

Fig. 5. Signal amplitudes of different roughness targets after compensation.

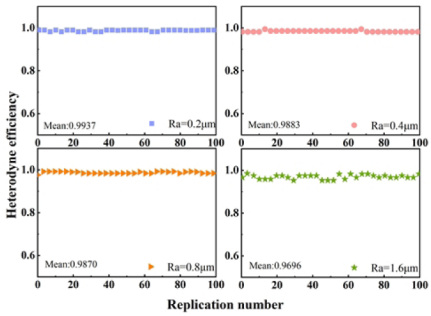

Fig. 6. Compensation results of HSA for heterodyne efficiency on different roughness targets.

Our analysis confirms the HSA algorithm's superiority in processing effectiveness, time efficiency, and stability. It effectively compensates for heterodyne array signals, rapidly enhancing overall detection system performance.

This paper introduces the integration of the heuristic search algorithm (HSA) into an active optical heterodyne detection system with a phase compensation algorithm scheme. Heterodyne experiments were conducted using four shot peening comparison samples with varying roughness levels as targets. Figure 5 showcases the heterodyne signals of these targets after algorithm processing, revealing significant improvements in spectral distribution compared to Fig. 2. Notably, the original signal spectrum experienced an impressive amplification of approximately 60 times for the comparison sample block with $Ra = 1.6\,\mu m$ (compared with the frequency spectrum before algorithm compensation in Fig. 2). The HSA algorithm facilitated real-time signal correction and processing, transforming the timing superposition of each pixel signal from ordinary to coherent. This highlights the algorithm's capability to achieve real-time signal processing, effectively enhancing the SNR of the echo signal.

The HSA algorithm processes signals from the array detector, with heterodyne efficiency evaluated over 100 iterations. Figure 6 reveals an average efficiency of 0.9937 for $Ra = 0.2\,\mu m$, approaching the ideal value. Without correction, direct superposition yields a low efficiency of 0.039. HSA exhibits superior stability when compensating for $Ra = 0.2\,\mu m$ rough surfaces. However, as roughness increases to $Ra = 1.6\,\mu m$, efficiency slightly decreases, potentially due to polarization and spot matching. Future investigations should address these factors to enhance the method's performance.

This research introduces an innovative approach for establishing an active coherent detection system that generates coherent interference signals on a camera sensor's photosensitive surface. The study thoroughly assesses the swarm intelligence algorithm's performance and limitations while proposing HSA as a more precise and stable alternative. HSA effectively addresses computational challenges with a large number of array elements, significantly boosting processing speed. Experimental validation using shot peened samples demonstrates the method's effectiveness in countering decoherence from rough target surfaces in heterodyne detection. By considering parameters like heterodyne efficiency, the system's progressive nature is confirmed, providing a robust foundation for practical applications in active light detection.

Funding. 111 Project (B17035); State Key Laboratory of Laser Interaction with Matter (SKLLIM2103); Natural Science Foundation of Shaanxi Province (2020JM-206).

Disclosures. The authors declare no conflicts of interest.

Data availability. Data underlying the results presented in this paper are not publicly available at this time but may be obtained from the authors upon reasonable request.

REFERENCES

1. T. Okoshi and K. Kikuchi, J. Opt. Commun. **2**, 3 (1981).
2. M. Bashkansky, R. L. Lucke, and E. Funk, *et al.*, Opt. Lett. **27**, 1983 (2002).
3. Y. Liu, X. Zeng, and C. Cao, *et al.*, Opt. Lett. **44**, 5896 (2019).
4. E. Baumann, J.-D. Deschênes, and F. R. Giorgetta, *et al.*, Opt. Lett. **39**, 4776 (2014).
5. D. Fink and S. N. Vodopia, Appl. Opt. **15**, 453 (1976).
6. P. K. Chan and K. D. Killinger, Opt. Lett. **16**, 1219 (1991).
7. H. Dong, G. Li, and R. Yang, *et al.*, Opt. Commun. **371**, 19 (2016).
8. H. Dong, G. Li, and M. Ao, *et al.*, Opt. Laser Technol. **105**, 139 (2018).
9. Y. Liu, X. Zeng, and C. Cao, *et al.*, Opt. Commun. **458**, 124812 (2020).
10. Y. Liu, M. Gao, and X. Zeng, *et al.*, Opt. Laser Eng. **146**, 106694 (2021).
11. Y. Liu, M. Zheng, and M. Xu, *et al.*, Opt. Express **30**, 1651 (2022).
12. F. Le Clerc, L. Collot, and M. Gross, Opt. Lett. **25**, 716 (2000).
13. M. Ajub, K. P. Chan, and N. Tanno, Opt. Rev. **9**, 170 (2002).
14. M. Akiba, K. P. Chan, and N. Tanno, Opt. Lett. **28**, 816 (2003).